Graphene Composites

DOI: 10.1002/anie.201308013

Metal Oxide-Coated Three-Dimensional Graphene Prepared by the Use of Metal–Organic Frameworks as Precursors**

*Xiehong Cao, Bing Zheng, Xianhong Rui, Wenhui Shi, Qingyu Yan, and Hua Zhang**

Abstract: *A simple method for the preparation of metal-oxide-coated three-dimensional (3D) graphene composites was developed. The metal–organic frameworks (MOFs) that served as the precursors of the metal oxides were first synthesized on the 3D graphene networks (3DGNs). The desired metal oxide/3DGN composites were then obtained by a two-step annealing process. As a proof-of-concept application, the obtained ZnO/3DGN and Fe_2O_3/3DGN materials were used in a photocatalytic reaction and a lithium-ion battery, respectively. We believe this method could be extended to the synthesis of other metal oxide/3DGN composites with 3D structures simply through the appropriate choice of specific MOFs as precursors.*

Owing to its unique structure and properties, graphene, a two-dimensional (2D) sp^2-hybrized carbon sheet, has been widely investigated.[1] Moreover, composites of graphene with many nanomaterials have been successfully prepared by various methods. Such composites exhibit improved properties and/or enhanced performance as compared to each individual component in the composite,[2] since the graphene sheet acts not only as a template or substrate with a large surface area for anchoring nanomaterials, but also as an electrically conductive channel for fast electron transfer.[3] Recently, three-dimensional (3D) graphene-based composites have attracted increasing interest, since they are not only electrically conductive, but also macroscopically porous, thus allowing ready access by gas molecules or electrolyte ions.[4] For example, 3D graphene networks (3DGNs)[5] synthesized by chemical vapor deposition (CVD) have exhibited high thermal conductivity[6] and good electrical and mechanical properties.[5a,7] Furthermore, the obtained 3DGNs can also be used as templates for the growth of various nanomaterials, such as oxides, sulfides, hydroxides, and carbon nanotubes.[8] However, the morphologies of reported metal oxide/3DGN composites normally showed that the 3DGNs were coated with thick films of metal oxide particles, rods, or flakes. To the best of our knowledge, until now there has been no report on the preparation of porous metal oxide nanostructures coated on 3DGNs without agglomeration.

Metal–organic frameworks (MOFs) that exhibit unique characteristics have been widely studied.[9] Composites of MOF and graphene oxide (GO), referred to as MOF/GO, in which the GO serves as a matrix for the well-dispersed growth of nanosized MOF crystals,[10d] have been synthesized.[10] Furthermore, when the GO was reduced, the reduced graphene oxide (rGO) obtained overcame the poor electrical conductivity of the MOF; thus, MOF/rGO composites can be used as promising electrode materials for electrocatalysis.[11] Herein, we report a simple method for the synthesis of metal oxides on 3DGNs. The application of the resulting materials, i.e. metal oxide/3DGN composites, in photocatalysis and lithium-ion batteries (LIBs), was also explored.

By using our simple method, a 3DGN (see Figure S1 in the Supporting Information),[5b] a porous 3D graphene structure, was used as a template for the preparation of the MOF/3DGN composite (Figure 1a, step 1). After annealing of the MOF/3DGN composite first under argon and then in air (Figure 1a, steps 2 and 3), the metal oxide/3DGN composite was obtained. As a proof of concept, the well-known MOFs ZIF-8[12] and MIL-88-Fe[13] were used for the preparation of ZnO/3DGN and Fe_2O_3/3DGN composites, respectively. As a result of the unique properties of 3DGNs,[5] the metal oxide/3DGN composites were electrically conductive and also possessed good mechanical properties (Figure 1b–e).

Figure 2a shows the morphology of the 3DGN after the growth of ZIF-8: ZIF-8/3DGN exhibited a rougher surface as compared to that of the original 3DGN (see Figure S1b). The crystal structure of ZIF-8 was confirmed by X-ray diffraction (XRD; see Figure S2).[12,14] Energy-dispersive X-ray spectroscopy (EDX) also indicated the presence of elemental zinc (see Figure S3). ZIF-8 nanocrystals with a polygonal shape and a size of approximately 500 nm were coated on the surface of the 3DGN (Figure 2b). By changing the synthetic conditions, the size of the ZIF-8 nanocrystals could be tuned from about 100 to about 900 nm (see Figure S4).

After annealing of the ZIF-8/3DGN composite under argon gas, the surface of the obtained sample was more textured and rougher (Figure 2c). Nanoparticles (NPs) with a size of approximately 10 nm were generated (Figure 2d). Selected-area electron diffraction (SAED) pattern indicated

[*] X. Cao,[+] B. Zheng,[+] X. Rui, W. Shi, Prof. Q. Yan, Prof. H. Zhang
School of Materials Science and Engineering
Nanyang Technological University
50 Nanyang Avenue, Singapore 639798 (Singapore)
E-mail: HZhang@ntu.edu.sg
hzhang166@yahoo.com
Homepage: http://www.ntu.edu.sg/home/hzhang/

[+] These authors contributed equally.

[**] This project was supported by Singapore MOE under AcRF Tier 2 (ARC 10/10, No. MOE2010-T2-1-060; ARC 26/13, No. MOE2013-T2-1-034), and AcRF Tier 1 (RG 61/12, RGT18/13), and Start-Up Grant M4080865.070.706022. This research was also funded by the Singapore National Research Foundation, and publication was supported by the Campus for Research Excellence and Technological Enterprise (CREATE) program "Nanomaterials for Energy and Water Management".

Supporting information for this article is available on the WWW under http://dx.doi.org/10.1002/anie.201308013.

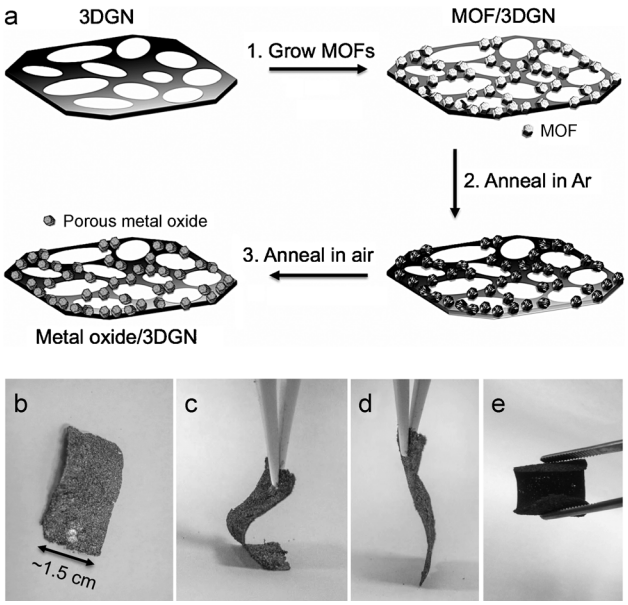

Figure 1. Preparation of metal oxide/3DGN composites. a) Schematic illustration of the process used for the synthesis of metal oxide/3DGN composites. b–d) Photographs of the ZnO/3DGN composite as obtained (b), under bending (c), and after the release of pressure (d). e) Photograph of the obtained Fe_2O_3/3DGN composite under bending.

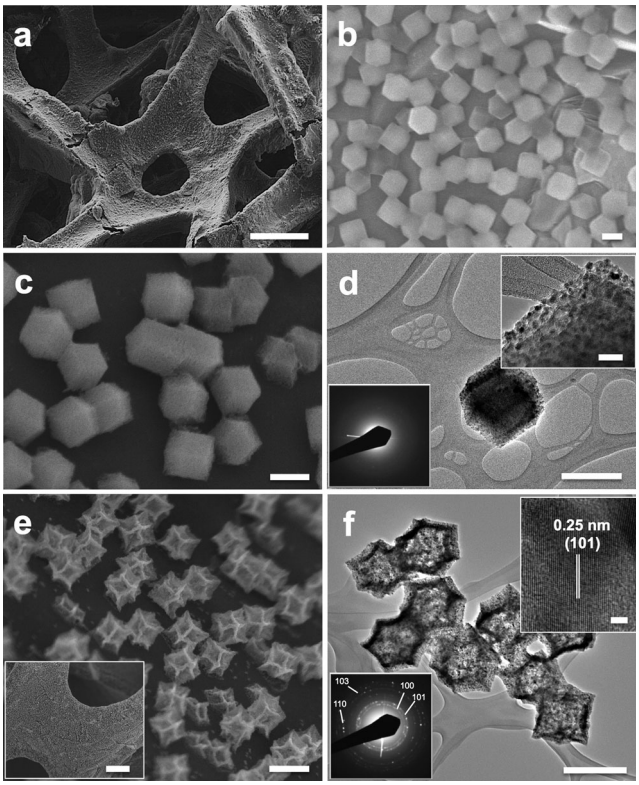

Figure 2. SEM and TEM images of ZIF-8/3DGN and ZnO/3DGN composites. a) Low- (scale bar: 100 μm) and b) high-magnification SEM images (scale bar: 500 nm) of the ZIF-8/3DGN composite. c) SEM image of the ZIF-8/3DGN composite after annealing under Ar (scale bar: 500 nm). d) TEM image of the annealed ZIF-8 nanocrystals in (c) (scale bar: 500 nm). Inset: High-magnification TEM image (top; scale bar: 30 nm) and SAED pattern (bottom) of an annealed ZIF-8 nanocrystal. e) SEM image of the ZnO/3DGN composite (scale bar: 500 nm). Inset: Low-magnification SEM image of the ZnO/3DGN composite (scale bar: 20 μm). f) TEM image of the porous ZnO structures in (e) (scale bar: 500 nm). Inset: HRTEM image of a ZnO NP (top; scale bar: 2 nm) and SAED pattern of the porous ZnO structure (bottom).

that these NPs have an amorphous structure (bottom inset of Figure 2d). Raman spectra showed that the intensity of the D-band increased after annealing of the ZIF-8/3DGN composite in argon (see Figure S5), thus suggesting that the organic component of ZIF-8 was converted into amorphous carbon coated on the surface of the NPs. The amorphous carbon could serve as a buffer that impedes the further contraction of ZIF-8 nanocrystals during annealing.[15]

Figure 2e,f shows the porous metal oxide/3DGN composite obtained after subsequent heat treatment of the sample in Figure 2c in air. The obtained porous metal oxide structures were a bit smaller than the ZIF-8 nanocrystals obtained after annealing in argon (Figure 2c). This difference in size can be attributed to the decomposition of amorphous carbon in the sample in Figure 2c during annealing in air and the contraction of the metal oxide structure during the cooling process.

The XRD pattern, high-resolution TEM (HRTEM), and the SAED pattern further confirmed that the porous metal-oxide structure coated on the 3DGN was composed of ZnO NPs. The XRD pattern (see Figure S6) showed the distinct (100), (002), and (101) diffraction peaks of ZnO, thus indicating that the hexagonal phase of ZnO (JCPDS 79-0205) was formed.[16] The HRTEM image of a small ZnO particle (top inset of Figure 2f) shows a lattice spacing of approximately 0.25 nm, which matches the (101) plane of ZnO. Four clear diffraction rings were observed in the SAED pattern (bottom inset of Figure 2f) and can be assigned to the (100), (101), (110), and (103) planes of ZnO, respectively.

Thus, a novel ZnO/3DGN composite was obtained by using the MOF ZIF-8 as the precursor of ZnO and a 3DGN as the 3D template. Moreover, since the size of the ZIF-8 nanocrystals growing on 3DGNs can be tuned by changing the synthetic conditions (see Figure S4a,c,e), the size of the porous ZnO structures in ZnO/3DGN composites can also be tuned (see Figure S4b,d,f). Although a ZIF-8 with a small size of approximately 100 nm could be synthesized on a 3DGN (see Figure S4g), only ZnO NPs rather than porous ZnO structures were obtained after the two-step annealing process (see the inset in Figure S4h).

As another sample, a Fe_2O_3/3DGN composite was also obtained after two-step annealing of MIL-88-Fe/3DGN (Figure 1a; see details in the Experimental Section). MIL-88-Fe was successfully coated on the surface of a 3DGN to form a MIL-88-Fe/3DGN composite (Figure 3a). The crystal structure of MIL-88-Fe was confirmed by XRD (see Figure S7a). In the obtained Fe_2O_3/3DGN composite (Figure 3b), the presence of α-Fe_2O_3 was confirmed on the basis of the SAED pattern, HRTEM, and XRD (Figure 3c,d; see also Figure S7b). The SAED pattern shows four clear diffraction rings, which can be assigned to the (012), (104), (110), and (113) planes of α-Fe_2O_3 (Figure 3c, inset). A lattice spacing of approximately 0.25 nm corresponding to the (110)

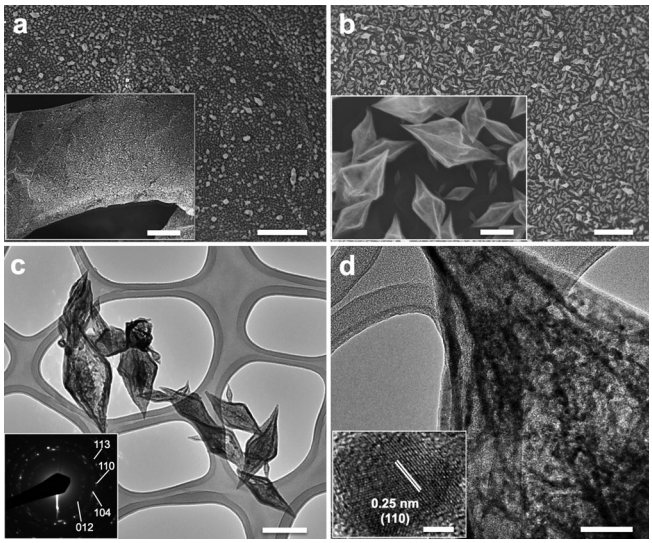

Figure 3. SEM and TEM images of MIL-88-Fe/3DGN and Fe_2O_3/3DGN composites. a) SEM image of the MIL-88-Fe/3DGN composite (scale bar: 5 μm). Inset: Low-magnification SEM image of the MIL-88-Fe/3DGN composite (scale bar: 10 μm). b) SEM image of the Fe_2O_3/3DGN composite (scale bar: 3 μm). Inset: High-magnification SEM image of the Fe_2O_3/3DGN composite (scale bar: 200 nm). c,d) TEM images of Fe_2O_3 structures (scale bars: 200 (c) and 50 nm (d)). Insets: SAED pattern (c) and HRTEM image (d) of Fe_2O_3 (scale bar: 2 nm).

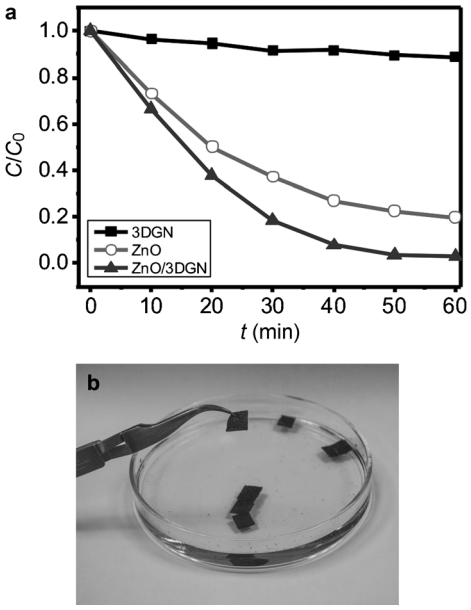

Figure 4. Photocatalytic properties of ZnO, 3DGN, and the ZnO/3DGN composite. a) Photocatalytic performance of the ZnO/3DGN composite, the 3DGN, and ZnO in the degradation of methylene blue. b) Photograph of the washing of ZnO/3DGN composites after the photodegradation process.

plane of α-Fe_2O_3 was observed in the HRTEM image (Figure 3d, inset).[17]

ZnO is an important photocatalyst owing to its low cost, nontoxic nature, and high photochemical activity.[18] In this study, the photocatalytic properties of the ZnO/3DGN composite were examined through the photodegradation of the dye methylene blue (MB) under irradiation with UV light. For comparison, the pure 3DGN and ZnO, which was obtained by the two-step annealing of ZIF-8 (see Figure S8), were used in control experiments.

Figure 4a shows the normalized change in the concentration of MB (C/C_0) during the photodegradation process; C and C_0 are the measured concentration of MB after photodegradation for a certain time and the original concentration of MB, respectively. It is evident that the ZnO/3DGN composite exhibited better photodegradation performance than did the pure 3DGN and ZnO. After irradiation of the dye solution with the 3DGN, ZnO, or ZnO/3DGN for 60 min, almost all of the dye was decomposed by ZnO/3DGN, whereas only about 12 and 80% of the dye was decomposed by the 3DGN and ZnO, respectively (Figure 4a). The improved performance could be attributed to the high surface area of the ZnO/3DGN composite and prevention of the recombination of photoinduced holes and electrons owing to the good contact and effective interaction between the 3DGN and ZnO (see Figure S9).

Recycling of the ZnO/3DGN composite was quite convenient as a result of the good mechanical properties and robust structure of the 3DGN (Figure 1). After the photodegradation process, the ZnO/3DGN composite could be picked up easily from the dye solution with tweezers, then washed thoroughly in Milli-Q water (Figure 4b) and dried for the subsequent photodegradation experiments. The durability of the ZnO/3DGN composite was tested (see Figure S10). After four consecutive cycles, there was no obvious change in its photodegradation performance, thus indicating the good stability of the photocatalytic properties of the ZnO/3DGN composite.

Fe_2O_3 is a promising anode material for lithium-ion batteries (LIBs).[19] The combination of Fe_2O_3 with graphene has been proved to further improve the lithium-storage properties, with higher specific capacities and better cycling stability.[20] In this study, the Fe_2O_3/3DGN composite was tested as the anode for LIBs, in which the 3DGN served as the current collector. The Fe_2O_3 powder used in the control experiment was synthesized by two-step annealing of MIL-88-Fe (see Figure S11) and then pasted on Cu foil with carbon black and a binder for LIB-anode testing. Figure 5a shows the first three discharge/charge curves for the Fe_2O_3/3DGN composite at a current density of 0.2 $A\,g^{-1}$ between 0.01 and 3 V (versus Li/Li^+). In the first discharge curve, the two sloping voltage plateaus at approximately 1.5 and 1.0 V can be ascribed to the structural transformation of Fe_2O_3 and the insertion of lithium ions, respectively.[19a] The voltage plateau at approximately 0.8 V corresponds to the conversion of $Li_2Fe_2O_3$ into Fe. This reaction is reversed in the subsequent charging process, as reflected by a sloping plateau at approximately 2.0 V in the first charge curve.[20a] These results are in good agreement with previous studies.[20,21] A small charge/discharge plateau found at about 0.1 V resulted from lithium intercalation/deintercalation between graphene layers.[22]

The cycling behavior of the Fe_2O_3/3DGN and Fe_2O_3 electrodes is compared in Figure 5b. After 50 discharge/charge cycles at the current density of 0.2 $A\,g^{-1}$, the Fe_2O_3

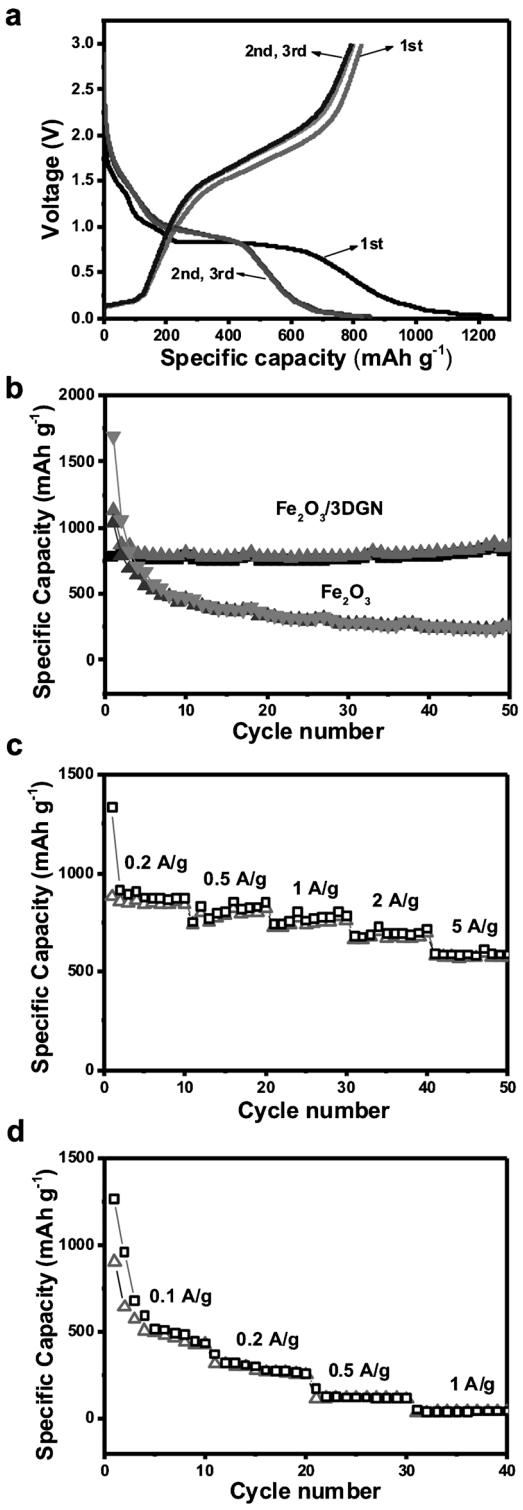

Figure 5. Lithium-ion-battery performance. a) Discharge/charge curves of the Fe_2O_3/3DGN composite. b) Cycling performance of the Fe_2O_3/3DGN composite and Fe_2O_3. c,d) Rate capacity of electrodes composed of the Fe_2O_3/3DGN composite (c) and Fe_2O_3 (d). Square and triangle symbols indicate the discharge and charge specific capacities, respectively.

electrode showed a fast decay of the capacity to 261 $mAh\,g^{-1}$ in the 50th cycle, whereas a reversible capacity as high as 864 $mAh\,g^{-1}$ was retained for the Fe_2O_3/3DGN composite (approximately 76% of the initial capacity of 1133 $mAh\,g^{-1}$), thus indicating good cyclability of the Fe_2O_3/3DGN composite.

The rate capacities of the electrodes were also measured. The Fe_2O_3/3DGN composite electrode exhibited 10th-cycle discharge capacities of 871, 854, 785, 718, and 587 $mA\,h\,g^{-1}$ at current densities of 0.2, 0.5, 1, 2, and 5 $A\,g^{-1}$, respectively (Figure 5c), thus implying a good rate performance. The capacity of the Fe_2O_3/3DGN composite at high current densities, such as 2 and 5 $A\,g^{-1}$, was comparable with and even higher than those of composites of iron oxides and graphene.[20b,21,23] In contrast, the Fe_2O_3 electrode provided a worse rate capacity (Figure 5d).

The areal density of 3DGNs (ca. 0.65 $mg\,cm^{-2}$) is much lower than that of the commonly used copper current collector (ca. 10 $mg\,cm^{-2}$).[24] This feature makes 3DGNs promising for the development of lightweight LIBs, as they enable the total weight of the electrode to be reduced and also provide high capacity per unit mass of electrode. For example, at a current density of 0.2 $A\,g^{-1}$, the Fe_2O_3/3DGN composite provided a capacity per gram of the electrode of 864 $mA\,h\,g^{-1}$ after 50 cycles, whereas only 24.3 $mA\,h\,g^{-1}$ was observed for the Fe_2O_3 electrode (as based on the total mass of the current collector, including active materials, a conductive additive, and a polymer binder).

In summary, we have developed a simple method to prepare novel metal oxide/3DGN composites by the use of MOFs as the precursors of the metal oxide and 3DGNs as the backbone through a facile two-step annealing process. As a proof of concept, the obtained ZnO/3DGN and Fe_2O_3/3DGN composites were used in photocatalysis and a lithium-ion battery (LIB). We believe this method could be used for the synthesis of other metal oxide/3DGN composites with 3D structures simply by the appropriate choice of a specific MOF as the precursor.

Experimental Section

Chemicals: Zinc nitrate ($Zn(NO_3)_2$), 2-methylimidazole (MIM, $C_4H_6N_2$), ferric chloride ($FeCl_3$), terephthalic acid (H2BDC, $C_8H_6O_4$), methanol, and *N*,*N*-dimethylformamide (DMF) were purchased from Sigma–Aldrich. All of the reagents were used without further purification.

Synthesis of ZIF-8 crystals: $Zn(NO_3)_2$ (100 $mmol\,L^{-1}$, 15 mL) and MIM (100 $mmol\,L^{-1}$, 30 mL) were stirred in methanol at room temperature for 12 h. The resulting ZIF-8 crystals were collected by centrifugation, then washed with methanol several times and dried in a vacuum oven at room temperature.

Synthesis of MIL-88-Fe crystals: A mixture of $FeCl_3$ (243 mg) and H2BDC (166 mg) in DMF (10 mL) was heated at 100 °C in an oil bath for 12 h and then allowed to cool naturally to room temperature. The resulting MIL-88-Fe crystals were collected by centrifugation, then washed with ethanol several times and dried in a vacuum oven at room temperature.

Synthesis of 3D graphene networks (3DGNs) by CVD: The preparation of 3DGNs was based on our previous work.[5b] Briefly, the nickel foam was annealed at 1000 °C for 10 min in a CVD chamber, which was filled with a mixture of the gases Ar (200 sccm) and H_2 (40 sccm). The furnace was then allowed to cool down naturally to 950 °C. When the temperature of the furnace was stable, ethanol was bubbled into the furnace tube with a flow of Ar (10 sccm) for 10 min. The furnace was then cooled down fast to room temperature at

a cooling rate of about 100 °C min^{-1}, and 3DGNs coated on Ni foam were obtained. For the preparation of a 3DGN electrode for LIBs, the graphene growth time was elongated to 60 min, and the furnace was allowed to cool down naturally to room temperature. To remove the Ni foam, the synthesized sample was first dipped into a solution of poly(methyl methacrylate) (PMMA; 4.5 wt% PMMA with a molecular weight of approximately 996000 in anisole) for several seconds. After the anisole had evaporated, the PMMA-coated sample was immersed in the etchant solution (mixture of $FeCl_3$ (1 mol L^{-1}) and HCl (2 mol L^{-1}) in water) at 60 °C to remove the Ni foam. Finally, the PMMA coated on the 3DGN was removed by hot acetone vapor and subsequent annealing at 450 °C under Ar (200 sccm) and H_2 (40 sccm).

Synthesis of ZIF-8/3DGN composites: Prior to the synthesis of MOF/3DGN composites, the 3DGN was first heated in 69 wt% HNO_3 at 80 °C overnight. The acid-treated 3DGN was then placed in a glass bottle, and menthol (1 mL) was added, followed by methanolic solutions of $Zn(NO_3)_2$ (100 mmol L^{-1}, 0.5 mL) and MIM (100 mmol L^{-1}, 1 mL). After 12 h, the ZIF-8/3DGN composite was picked up with tweezers, rinsed with methanol thoroughly, and dried in a vacuum oven at room temperature. The growth temperature and the concentration of the $Zn(NO_3)_2$ and MIM were tuned for the synthesis of ZIF-8/3DGN composites with various sizes of ZIF-8 coated on the 3DGN.

Synthesis of MIL-88-Fe/3DGN composites: $FeCl_3$ (243 mg) and H2BDC (166 mg) were first mixed in DMF (10 mL). Acid-treated 3DGN was immersed in the mixture, which was then heated at 100 °C in an oil bath for 12 h. The solution was allowed to cool down naturally to room temperature, and then the MIL-88-Fe/3DGN composite was picked up with tweezers, rinsed with ethanol, and dried in a vacuum oven at room temperature.

Synthesis of metal oxide/3DGN composites: The synthesized MOF/3DGN composite was placed in the center of a quartz tube and annealed under Ar protection with a gas flow rate of 250 sccm for 1 h at 450 °C. The annealed MOF/3DGN composite was subsequently heated in air for 1 h at 380 °C to give ZnO/3DGN or Fe_2O_3/3DGN.

Photocatalytic degradation of a dye: A suspension of the ZnO/3DGN composite (1.5 mg) and methylene blue (15 mL, 15 mg L^{-1}) was first stirred in the dark for 30 min and then irradiated with a full-spectrum xenon/mercury–xenon lamp (Hamamatsu Photonics K.K.). The concentration of methylene blue was calculated according to Beer's law on the basis of the absorption peak at 664 nm for methylene blue by using a UV-1800 UV/Vis spectrophotometer (Shimadzu).

Lithium-ion-battery measurements: A solution of $LiPF_6$ (1 mol L^{-1}) in ethylene carbonate/diethyl carbonate (1:1 in volume) was used as the electrolyte, and pure lithium foil was used as both the counter and the reference electrode in two-electrode coin cells. The galvanostatic discharge/charge measurements in the voltage window of 0.01–3 V were carried out with a Neware battery tester (BTS-5V5mA, Neware, China). The Fe_2O_3/3DGN composite was used directly as the working electrode, without the use of additional conductive materials or binders. In the control experiment, the Fe_2O_3 powder obtained by two-step annealing of MIL-88-Fe was used as the working electrode. To obtain the Fe_2O_3 electrode, a slurry prepared by mixing the Fe_2O_3 powder with poly(vinylidene fluoride) (PVDF) binder and conductive carbon black (8:1:1, weight ratio) was coated on Cu foil and dried in a vacuum oven.

Characterization: The morphologies of the samples were characterized by SEM (Model JSM-7600F, JEOL) and TEM (JSM-2010, JEOL). Raman spectra were collected with a WITec CRM200 Raman System (488 nm laser, 2.54 eV, WITec). XRD tests were performed on an XRD-600 X-ray diffractometer (Shimadzu).

Received: September 12, 2013
Revised: November 23, 2013
Published online: December 20, 2013

Keywords: composite materials · lithium-ion batteries · metal–organic frameworks · photocatalysis · three-dimensional graphene networks

[1] a) A. K. Geim, K. S. Novoselov, *Nat. Mater.* **2007**, *6*, 183 – 191; b) Y. Zhu, S. Murali, W. Cai, X. Li, J. W. Suk, J. R. Potts, R. S. Ruoff, *Adv. Mater.* **2010**, *22*, 3906 – 3924.

[2] a) X. Huang, X. Qi, F. Boey, H. Zhang, *Chem. Soc. Rev.* **2012**, *41*, 666 – 686; b) X. Huang, Z. Yin, S. Wu, X. Qi, Q. He, Q. Zhang, Q. Yan, F. Boey, H. Zhang, *Small* **2011**, *7*, 1876 – 1902; c) L. Huang, N. Yi, Y. Wu, Y. Zhang, Q. Zhang, Y. Huang, Y. Ma, Y. Chen, *Adv. Mater.* **2013**, *25*, 2224 – 2228; d) V. C. Tung, J. Kim, J. Huang, *Adv. Energy Mater.* **2012**, *2*, 299 – 303; e) B. Lung-Hao Hu, F.-Y. Wu, C.-T. Lin, A. N. Khlobystov, L.-J. Li, *Nat. Commun.* **2013**, *4*, 1687; f) K. Yang, L. Hu, X. Ma, S. Ye, L. Cheng, X. Shi, C. Li, Y. Li, Z. Liu, *Adv. Mater.* **2012**, *24*, 1868 – 1872.

[3] a) W. Shi, J. Zhu, D. H. Sim, Y. Y. Tay, Z. Lu, X. Zhang, Y. Sharma, M. Srinivasan, H. Zhang, H. H. Hng, Q. Yan, *J. Mater. Chem.* **2011**, *21*, 3422 – 3427; b) Y. Wang, X. Yang, L. Qiu, D. Li, *Energy Environ. Sci.* **2013**, *6*, 477 – 481; c) C. Peng, B. Jiang, Q. Liu, Z. Guo, Z. Xu, Q. Huang, H. Xu, R. Tai, C. Fan, *Energy Environ. Sci.* **2011**, *4*, 2035 – 2040.

[4] a) Y. Xu, Q. Wu, Y. Sun, H. Bai, G. Shi, *ACS Nano* **2010**, *4*, 7358 – 7362; b) J. Li, C.-y. Liu, Y. Liu, *J. Mater. Chem.* **2012**, *22*, 8426 – 8430; c) Z.-S. Wu, S. Yang, Y. Sun, K. Parvez, X. Feng, K. Müllen, *J. Am. Chem. Soc.* **2012**, *134*, 9082 – 9085; d) Y. Xu, X. Huang, Z. Lin, X. Zhong, Y. Huang, X. Duan, *Nano Res.* **2013**, *6*, 65 – 76; e) J. Yuan, J. Zhu, H. Bi, X. Meng, S. Liang, L. Zhang, X. Wang, *Phys. Chem. Chem. Phys.* **2013**, *15*, 12940 – 12945; f) L. Zhang, F. Zhang, X. Yang, G. Long, Y. Wu, T. Zhang, K. Leng, Y. Huang, Y. Ma, A. Yu, Y. Chen, *Sci. Rep.* **2013**, DOI: 10.1038/srep01408.

[5] a) Z. Chen, W. Ren, L. Gao, B. Liu, S. Pei, H.-M. Cheng, *Nat. Mater.* **2011**, *10*, 424 – 428; b) X. Cao, Y. Shi, W. Shi, G. Lu, X. Huang, Q. Yan, Q. Zhang, H. Zhang, *Small* **2011**, *7*, 3163 – 3168.

[6] M. T. Pettes, H. Ji, R. S. Ruoff, L. Shi, *Nano Lett.* **2012**, *12*, 2959 – 2964.

[7] Z. Chen, C. Xu, C. Ma, W. Ren, H.-M. Cheng, *Adv. Mater.* **2013**, *25*, 1296 – 1300.

[8] a) X. Cao, Z. Zeng, W. Shi, P. Yep, Q. Yan, H. Zhang, *Small* **2012**, *9*, 1703 – 1707; b) X. Cao, Y. Shi, W. Shi, X. Rui, Q. Yan, J. Kong, H. Zhang, *Small* **2013**, *9*, 3433 – 3438; c) W. Zhou, X. Cao, Z. Zeng, W. Shi, Y. Zhu, Q. Yan, H. Liu, J. Wang, H. Zhang, *Energy Environ. Sci.* **2013**, *6*, 2216 – 2221; d) F. Yavari, Z. Chen, A. V. Thomas, W. Ren, H.-M. Cheng, N. Koratkar, *Sci. Rep.* **2011**, DOI: 10.1038/srep00166; e) B.-J. Kim, G. Yang, M. J. Park, J. S. Kwak, K. H. Baik, D. Kim, J. Kim, *Appl. Phys. Lett.* **2013**, *102*, 161902 – 161904; f) J.-C. Yoon, J.-S. Lee, S.-I. Kim, K.-H. Kim, J.-H. Jang, *Sci. Rep.* **2013**, DOI: 10.1038/srep01788; g) H. Ji, L. Zhang, M. T. Pettes, H. Li, S. Chen, L. Shi, R. Piner, R. S. Ruoff, *Nano Lett.* **2012**, *12*, 2446 – 2451; h) X.-C. Dong, H. Xu, X.-W. Wang, Y.-X. Huang, M. B. Chan-Park, H. Zhang, L.-H. Wang, W. Huang, P. Chen, *ACS Nano* **2012**, *6*, 3206 – 3213.

[9] a) H. K. Chae, D. Y. Siberio-Pérez, J. Kim, Y. Go, M. Eddaoudi, A. J. Matzger, M. O'Keeffe, O. M. Yaghi, *Nature* **2004**, *427*, 523 – 527; b) G. Lu, S. Li, Z. Guo, O. K. Farha, B. G. Hauser, X. Qi, Y. Wang, X. Wang, S. Han, X. Liu, J. S. DuChene, H. Zhang, Q. Zhang, X. Chen, J. Ma, S. C. J. Loo, W. D. Wei, Y. Yang, J. T. Hupp, F. Huo, *Nat. Chem.* **2012**, *4*, 310 – 316; c) S. Hermes, M.-K. Schröter, R. Schmid, L. Khodeir, M. Muhler, A. Tissler, R. W. Fischer, R. A. Fischer, *Angew. Chem.* **2005**, *117*, 6394 – 6397; *Angew. Chem. Int. Ed.* **2005**, *44*, 6237 – 6241; d) S. L. James, *Chem. Soc. Rev.* **2003**, *32*, 276 – 288; e) R. J. Kuppler, D. J. Timmons, Q.-R. Fang, J.-R. Li, T. A. Makal, M. D. Young, D. Yuan, D. Zhao, W. Zhuang, H.-C. Zhou, *Coord. Chem. Rev.* **2009**, *253*, 3042 – 3066; f) L. E. Kreno, K. Leong, O. K. Farha, M.

Allendorf, R. P. Van Duyne, J. T. Hupp, *Chem. Rev.* **2011**, *111*, 1105 – 1125; g) B. Chen, N. W. Ockwig, A. R. Millward, D. S. Contreras, O. M. Yaghi, *Angew. Chem.* **2005**, *117*, 4823 – 4827; *Angew. Chem. Int. Ed.* **2005**, *44*, 4745 – 4749; h) Q.-R. Fang, G.-S. Zhu, Z. Jin, Y.-Y. Ji, J.-W. Ye, M. Xue, H. Yang, Y. Wang, S.-L. Qiu, *Angew. Chem.* **2007**, *119*, 6758 – 6762; *Angew. Chem. Int. Ed.* **2007**, *46*, 6638 – 6642; i) S. S. Han, W.-Q. Deng, W. A. Goddard, *Angew. Chem.* **2007**, *119*, 6405 – 6408; *Angew. Chem. Int. Ed.* **2007**, *46*, 6289 – 6292; j) J. Li, S. Cheng, Q. Zhao, P. Long, J. Dong, *Int. J. Hydrogen Energy* **2009**, *34*, 1377 – 1382; k) M. Tonigold, Y. Lu, B. Bredenkötter, B. Rieger, S. Bahnmüller, J. Hitzbleck, G. Langstein, D. Volkmer, *Angew. Chem.* **2009**, *121*, 7682 – 7687; *Angew. Chem. Int. Ed.* **2009**, *48*, 7546 – 7550; l) J. S. Seo, D. Whang, H. Lee, S. I. Jun, J. Oh, Y. J. Jeon, K. Kim, *Nature* **2000**, *404*, 982 – 986; m) G. J. Halder, C. J. Kepert, B. Moubaraki, K. S. Murray, J. D. Cashion, *Science* **2002**, *298*, 1762 – 1765.

[10] a) C. Petit, T. J. Bandosz, *Adv. Mater.* **2009**, *21*, 4753 – 4757; b) Z.-H. Huang, G. Liu, F. Kang, *ACS Appl. Mater. Interfaces* **2012**, *4*, 4942 – 4947; c) J. H. Lee, S. Kang, J. Jaworski, K.-Y. Kwon, M. L. Seo, J. Y. Lee, J. H. Jung, *Chem. Eur. J.* **2012**, *18*, 765 – 769; d) S. Liu, L. Sun, F. Xu, J. Zhang, C. Jiao, F. Li, Z. Li, S. Wang, Z. Wang, X. Jiang, H. Zhou, L. Yang, C. Schick, *Energy Environ. Sci.* **2013**, *6*, 818 – 823.

[11] M. Jahan, Q. Bao, K. P. Loh, *J. Am. Chem. Soc.* **2012**, *134*, 6707 – 6713.

[12] K. S. Park, Z. Ni, A. P. Côté, J. Y. Choi, R. Huang, F. J. Uribe-Romo, H. K. Chae, M. O'Keeffe, O. M. Yaghi, *Proc. Natl. Acad. Sci. USA* **2006**, *103*, 10186 – 10191.

[13] S. Bauer, C. Serre, T. Devic, P. Horcajada, J. Marrot, G. Férey, N. Stock, *Inorg. Chem.* **2008**, *47*, 7568 – 7576.

[14] Y. Pan, Y. Liu, G. Zeng, L. Zhao, Z. Lai, *Chem. Commun.* **2011**, *47*, 2071 – 2073.

[15] X. Xu, R. Cao, S. Jeong, J. Cho, *Nano Lett.* **2012**, *12*, 4988 – 4991.

[16] Z. Yin, S. Wu, X. Zhou, X. Huang, Q. Zhang, F. Boey, H. Zhang, *Small* **2010**, *6*, 307 – 312.

[17] M. F. Hassan, Z. Guo, Z. Chen, H. Liu, *Mater. Res. Bull.* **2011**, *46*, 858 – 864.

[18] Q.-P. Luo, X.-Y. Yu, B.-X. Lei, H.-Y. Chen, D.-B. Kuang, C.-Y. Su, *J. Phys. Chem. C* **2012**, *116*, 8111 – 8117.

[19] a) X.-L. Wu, Y.-G. Guo, L.-J. Wan, C.-W. Hu, *J. Phys. Chem. C* **2008**, *112*, 16824 – 16829; b) H.-J. Kim, K.-I. Choi, A. Pan, I.-D. Kim, H.-R. Kim, K.-M. Kim, C. W. Na, G. Cao, J.-H. Lee, *J. Mater. Chem.* **2011**, *21*, 6549 – 6555.

[20] a) X. Zhu, Y. Zhu, S. Murali, M. D. Stoller, R. S. Ruoff, *ACS Nano* **2011**, *5*, 3333 – 3338; b) Y. Su, S. Li, D. Wu, F. Zhang, H. Liang, P. Gao, C. Cheng, X. Feng, *ACS Nano* **2012**, *6*, 8349 – 8356.

[21] M. Zhang, B. Qu, D. Lei, Y. Chen, X. Yu, L. Chen, Q. Li, Y. Wang, T. Wang, *J. Mater. Chem.* **2012**, *22*, 3868 – 3874.

[22] A. Kumar, A. L. M. Reddy, A. Mukherjee, M. Dubey, X. Zhan, N. Singh, L. Ci, W. E. Billups, J. Nagurny, G. Mital, P. M. Ajayan, *ACS Nano* **2011**, *5*, 4345 – 4349.

[23] W. Wei, S. Yang, H. Zhou, I. Lieberwirth, X. Feng, K. Müllen, *Adv. Mater.* **2013**, *25*, 2909 – 2914.

[24] N. Li, Z. Chen, W. Ren, F. Li, H.-M. Cheng, *Proc. Natl. Acad. Sci. USA* **2012**, *109*, 17360 – 17365.

